Nonlinear Doping, Chemical Passivation and Photoluminescence Mechanism in Water-Soluble Silicon Quantum Dots by Mechanochemical Synthesis *

Si-Min Huang(黄思敏)[1,2], Bo Qian(钱波)[2**], Ruo-Xi Shen(沈若曦)[2], Yong-Lin Xie(谢永林)[2]

[1]*School of Materials Science and Engineering, Shanghai University, Shanghai 200444*

[2]*Inkjet Printing Technology Research Center, Printable Electronics Research Center, Suzhou Institute of Nanotech and Nanobionics, Chinese Academy of Sciences, Suzhou 215125*

(Received 7 November 2017)

A series of boron- and phosphorus-doped silicon wafers are used to prepare a series of doped silicon nanocrystals (nc-Si) by high-energy ball milling with carboxylic acid-terminated surface. The sizes of the nc-Si samples are demonstrated to be <5 nm. The doping levels of the nc-Si are found to be nonlinearly dependent on the original doping level of the wafers by x-ray photoelectron spectroscopy measurement. It is found that the nonlinear doping process will lead to the nonlinear chemical passivation and photoluminescence (PL) intensity evolution. The doping, chemical passivation and PL mechanisms of the doped nc-Si samples prepared by mechanochemical synthesis are analyzed in detail.

PACS: 68.35.bg, 68.55.Ln, 81.05.Hd, 81.07.Bc DOI: 10.1088/0256-307X/35/3/036801

Incorporating a dopant element into silicon nanocrystals (nc-Si) and quantum dots (QD) is still one of the key technical challenges for the use of these materials in a number of optoelectronic applications.[1–4] There are many ways to prepare doped silicon nanocrystals, such as non-thermal plasma synthesis,[5,6] plasma enhanced chemical vapor deposition,[7] and laser ablation.[8] However, the doping mechanism remains complicated and needs further research. Unlike doping of traditional bulk semiconductor materials, the location of the doping element in silicon nanocrystals can be within the crystal lattice, on the surface, or within the surrounding matrix, which strongly depends on the preparation methods.

Understanding the doping mechanism is fundamental and very important in studying the doped nanocrystals. In this Letter, we try to use high-energy ball milling to prepare a series of doped silicon nanocrystals to investigate the influence of the original silicon wafer doping levels to the doping mechanism of the silicon quantum dots. Since the method is used at room temperature, the dopant element has the possibility to locate inside and on the surface. To the best of our knowledge, although high-energy ball milling is an efficient way to prepare nanocrystals,[9] there has been no systematical research on the doping mechanism of nc-Si based on this method.

We study the doping, chemical passivation and PL properties of a series of n- and p-type nc-Si samples prepared by mechanochemical synthesis. The nonlinear relationship of the doping levels between the doped nc-Si and the doped silicon wafers can be observed, as well as the chemical passivation and the PL intensity evolution. All the samples exhibit double-peak ultraviolet PL features at the similar wavelength positions. The oxygen and carbon related bonds are found to play important roles in structural and optical properties of nc-Si samples.

Silicon wafers (single side polished, ⟨100⟩) were purchased from Hangzhou JingBo Science and Technology Ltd. To prepare nc-Si with different doping levels, a series of doped silicon wafers were selected. There were three kinds of n-type silicon wafers with resistivities of 0.001–0.006 Ω·m (named as N1), 0.1–1 Ω·m (N2), and >3000 Ω·m (N3), respectively. For three kinds of p-type silicon wafers, the resistivities were 0.001–0.009 Ω·m (P1), 1–5 Ω·m (P2), and 10–20 Ω·m (P3), respectively. Note that for the convenience of expression, N1–N3 and P1–P3 were directly used to name the nc-Si prepared from the corresponding doped silicon wafers. For comparison, intrinsic silicon wafers with resistivity >10000 Ω·m were also purchased. All chemicals, including undecylenic acid and ethyl alcohol, were purchased from Sinopharm Chemical Reagent Co., Ltd.

The disco automatic dicing saw was used to cut the doped silicon wafers into dices ($2 \times 2\,\mathrm{mm}^2$). A 1.5 g of silicon pieces were placed in a stainless steel milling vial with two stainless steel milling balls (diameter of 1.2 cm, weighing approximately 8.1 g). In a glovebox under argon atmosphere, the vial was loaded, filled with approximately 37.5 ml undecylenic acid for 12 h, and then tightly sealed. After that, the milling vial was placed in an SPEX 8000-M dual mixer/mill, and milling for 24 h. After the milling was completed, the nanoparticle solutions were transferred to a plastic centrifugation tube and centrifuged for 15 min at 3000 rpm to remove large particles. Finally, the clear supernatant was placed in a vacuum oven for solvent removal to obtain the passivated silicon nanoparticles.

The detailed microstructures of the samples were performed by transmission electron microscopy

*Supported by the National Natural Science Foundation of China under Grant No 61575216.

**Corresponding author. Email: bqian2010@sinano.ac.cn

© 2018 Chinese Physical Society and IOP Publishing Ltd

(TEM, Tecnai G2 F20). Fourier transform infra-red (FTIR) spectra were measured by a Thermo Nicolet NEXUS 670 FTIR instrument. The UV-vis absorption was recorded using an ultraviolet/visible/near infrared spectrometer (Jasco V-660, Jasco, Japan). The excitation-emission spectra and photoluminescence data in the range of 200–900 nm were measured on a Hitachi F4600 spectrofluorimeter. For UV-vis and PL analyses, the nanoparticles were redissolved in ethyl alcohol. The x-ray photoelectron spectroscopy (XPS) measurements were performed on a Thermo Scientific ESCALAB 250Xi.

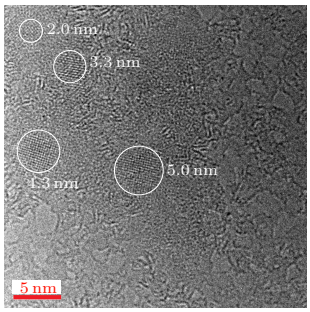

Fig. 1. The high-resolution transmission electron microscopy of nc-Si prepared from N2 by high energy ball milling. The nc-Si is marked by white circles. The measured sizes of nc-Si are also marked close to the nc-Si.

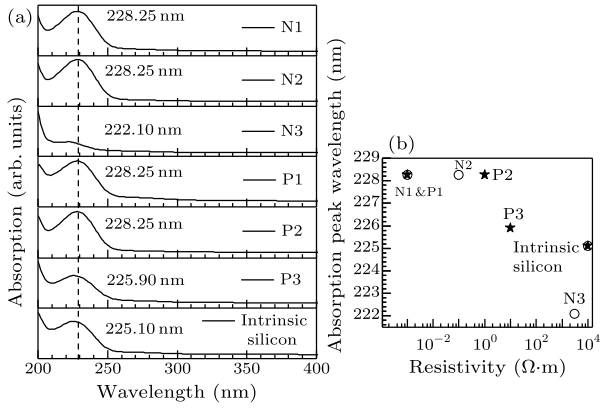

Fig. 2. (a) The absorption spectra of the nc-Si samples prepared from silicon wafers with different doping levels. (b) The relation between absorption peak wavelengths of nc-Si with the resistivity of the original silicon wafer.

Figure 1 illustrates the high-resolution transmission electron microscopy (HRTEM) of nc-Si prepared from N2. It can be clearly observed that nc-Si with the size from 2 nm to 5 nm was obtained, which can be considered as a silicon quantum dot. The absorption spectra of series doped nc-Si in the range of 200–400 nm are presented in Fig. 2(a). Generally, the absorption spectra for all the samples show clear Gaussion-like single bands. It can be observed that for the nc-Si prepared from the rather highly doped silicon wafers of N1, N2, P1, and P2, with the resistivity smaller than several Ω·m, the absorption spectrum peak wavelengths are almost the same, which are about 228.25 nm. For nc-Si prepared from the rather lower doped silicon wafers of N3, P3 and intrinsic silicon, the absorption spectrum peak wavelengths are 222.10 nm, 225.90 nm, and 225.10 nm, respectively. The more distinct comparison of the absorption peak wavelengths is illustrated in Fig. 2(b). The n-type samples are represented by empty circles. The p-type samples are represented by five-pointed stars. The data of the nc-Si prepared from the intrinsic silicon wafer are represented by both empty circle and five-pointed star. It is shown that for the doped nc-Si, with decreasing the resistivity of silicon wafer, the absorption peak wavelength increases and becomes saturated when the resistivity of the silicon wafer reaches several Ω·m. However, the absorption peak wavelength for the intrinsic sample is also smaller than the saturated wavelength. This means that the nc-Si preparation method by high energy ball milling of different doped silicon wafers will possibly change the bandgap of nc-Si.

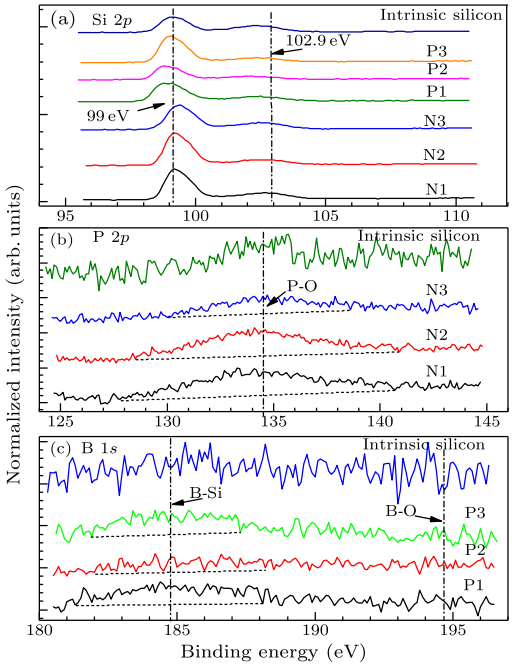

Fig. 3. XPS spectra: (a) Si 2*p*, (b) P 2*p* and (c) B 1*s* peaks for the nc-Si prepared from silicon wafers with different doping levels. The dash-dotted lines and dashed lines are drawn for the eye guiding of the peak positions and amplitude.

To understand the doping behaviors of the nc-Si prepared from the different doped wafers, XPS measurements were performed. It can be distinguished in Fig. 3(a) that there are two peaks for all the samples. For p-type samples, the two peaks are around 98.9 eV and 102.4 eV, respectively. For n-type samples, the two peaks are around 99.3 eV and 102.6 eV. The peaks around 98.5 eV are associated with Si^0, while the peaks around 102.9 eV are associated with Si^{4+}.[7] It can be deduced that the peak shift from n-type samples to p-type samples is probably due to the impurity atoms from different dopings which lead to the change of the Si bond strength. It also indicates

that the nc-Si is successfully doped.

In Fig. 3(b), there is only one peak located around 134.5 eV, which is related to the P–O bond[7,10] and can be observed for each n-type sample. There is no signal related to the P–Si bond, which should locate around 128.4 eV.[7,10] The lack of the P–Si bond in Fig. 3(b) also indicates that almost all of the original doped phosphorous atoms come out from the nc-Si by the size-dependent dopant self-purification effect,[11,12] while the presence of P–O bonds suggests that phosphorous prefers the surface of the nc-Si.[13] For the intensity of the P–O peak, N1 and N2 are almost the same, while N3 is smaller. This indicates that increasing the original doping level of the n-type silicon wafer may increase the possibility for the dopant atoms to occupy the surface of nc-Si.

Figure 3(c) presents the XPS spectra of the p-type nc-Si. The results of the intrinsic samples are presented as a reference. It is shown that peaks are around 184.7 eV. It indicates that there is B–Si bonding in the nc-Si.[14] Note that there are some small signals around 194.6 eV related to the B–O bond, whereas the intensity is much lower than the peak of the B–Si bond. This indicates that the boron prefers to concentrate within the nc-Si,[14,15] which is very different from the n-type nc-Si samples in Fig. 3(b). For the intensity of the B–Si peak, P1 and P3 are almost the same, while P2 is obviously smaller than the other two samples. It is well-known that the bandgap of the nanocrystals will increase with decreasing the size due to the quantum confinement effect. Meanwhile, the localized deep impurity level should not be affected as much by quantum confinement. This means that the energy levels of dopant become deeper for smaller nanocrystals, while the dopant will be less stable in the small nanocrystals. We tentatively suggest that when increasing the concentration of the original silicon wafer, the instability of dopant in nc-Si will also increase, since the ratio between unstable B–Si bonds and stable Si–Si bonds increases. This can probably explain why the XPS intensity of the B–Si bond of P2 is smaller than P3.

Figure 4 illustrates the FTIR spectra of nc-Si samples prepared from the doped wafers. There are six typical absorption bands observed, which are related to Si–O–Si (1084.03 cm^{-1}), Si–C (1262.61 cm^{-1}), $–CH_3$ (1441.18 cm^{-1}), $–CH_2$ (2934.87 cm^{-1}), C=C stretching (1596.64 cm^{-1} for n-type samples, 1544.12 cm^{-1} for p-type samples), $C=O$ (1710.08 cm^{-1} for n-type samples, 1665.97 cm^{-1} for p-type samples). The intensity of the Si–O–Si absorption band is the strongest for each sample. It is indicated that oxygen has a large opportunity to incorporate into the nc-Si. Since a great deal of attention has been paid to keeping away from the oxygen during the preparation process and the carbon related absorption intensity is much lower than that of the Si–O–Si bond, we suggest that there are many Si dangling bonds generated, and the surface of the nc-Si was only partly passivated by the carboxylic acid after ball milling, which lead to the oxidation after taking the samples out of the sealed milling vial. Note that Si–O–Si signals can also be observed in the report for the similar carboxylic acid-terminated silicon nanocrystals.[16] It is interesting to observe that the intensity of the Si–O–Si band of nc-Si is not linearly dependent on the Si wafer doping level.

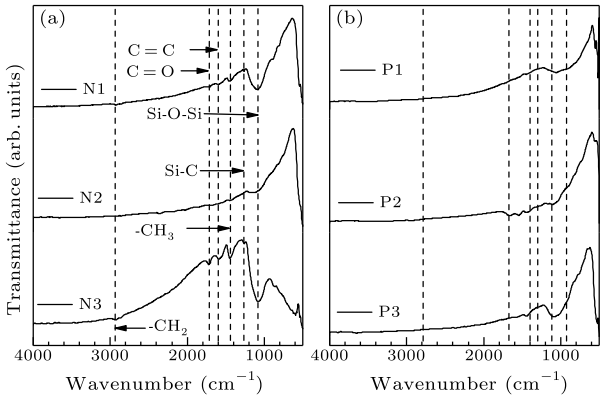

Fig. 4. FTIR spectra of n- (a) and p-type (b) of nc-Si samples. The dashed lines are drawn for the eye guiding of the absorption peaks.

According to the above results, especially in Figs. 3 and 4, we suggest that the nonlinear doping behavior of phosphorous and boron will lead to the nonlinear chemical passivation of nc-Si by mechanochemical synthesis, which is very different from the nc-Si prepared from pure silicon.[9] We tentatively propose two assumptions of the influence of the doping impurities in silicon wafer on the formation of nc-Si by mechanochemical synthesis. The first assumption is that the doping impurity close to or on the surface will hinder or disturb the formation of the carbon related bonds on the surface of nc-Si as well as the Si–O–Si bond, due to the coulomb force coming from the doping impurities. The second assumption is that after the impurities come out from the nc-Si during the high energy ball milling,[11,12] silicon dangling bonds will be left on the original doping sites of the nc-Si. Because the ball milling is at room temperature, there is no energy to reduce the silicon dangling bonds. It is also because the carbon related bonds can only form at the surface of the nc-Si.

Figure 5(a) shows the PL results of all the doped nc-Si samples. The nc-Si samples prepared from intrinsic silicon is also shown as a reference. The PL spectra are excited by an Xe lamp at 250 nm, which is close to the absorption band edges of all the samples as shown in Fig. 2. The measured PL spectrum range is from 280 nm to 480 nm. It is shown that most of the PL bands of all the samples are in the ultraviolet range (<400 nm). The spectra of all the samples can be fitted by two Gaussian peaks, and marked by peaks I and Ⅱ as shown in Fig. 5(a). The wavelength position and line width of two fitted peaks are close and similar between each sample in Fig. 5(a), including the nc-

Si prepared from intrinsic wafer. This indicates that there are two possible radiative recombination centers, and the doped impurities such as phosphorous and boron should not be the candidates of the possible radiative recombination center. It can also be observed that peak I is always narrower than peak Ⅱ according to the full width at half maximum (FWHM) as shown in Fig. 5(a).

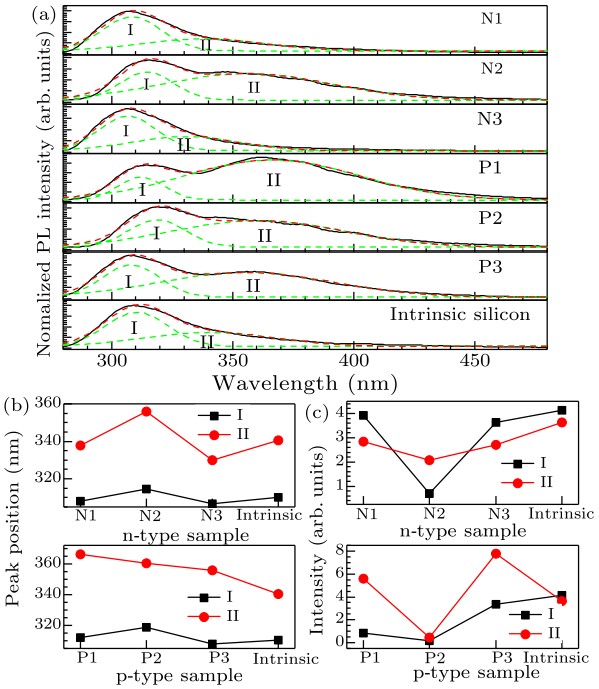

Fig. 5. (a) PL spectra of the nc-Si prepared from silicon wafers with different doping levels. The PL results of the intrinsic samples are shown as a reference in the bottom inset. Dashed green lines are multi-peaks Gaussian fitting curves, while dashed red lines correspond to the final Gaussian fitting to simulate the experimental data. Based on the fitted peaks in (a), (b) the peak positions and (c) the integrated PL intensities (not normalized) of n- and p-type samples are illustrated, respectively. The data for fitted peaks I and Ⅱ are presented by square dots and circle dots, respectively.

The evolution details of the peak position and integrated intensity (not normalized) of the two Gaussian fit peaks in Fig. 5(a) are shown in Fig. 5(b) and 5(c), respectively. From the upper inset in Fig. 5(b) for n-type samples, it can be observed that the trend of peak position evolution is the same for peaks I and Ⅱ. The PL peaks red shift from N1 to N2, then blue shift from N2 to N3, finally red shift from N3 to the intrinsic sample. The wavelength shift amplitude of peak I is larger than that of peak Ⅱ. From the bottom inset in Fig. 5(b), for p-type samples, it can be observed that the trend of peak position evolution is different between peaks I and Ⅱ. The trend of peak Ⅱ of p-type samples is the same as the n-type samples, while peak I appears with a continuous blue shift from P1 to the intrinsic sample. Since the absorption band peaks are saturate for highly doped samples as shown in Fig. 2, the nonlinear change of the fit PL peak position is probably originated from the change of the recombination energy level due to the detail structure difference of the nc-Si as shown in Figs. 3 and 4.

In Fig. 5(c), the evolution trends are almost the same for all the curves, except from P3 to the intrinsic sample for peak Ⅱ of p-type samples. The PL intensity change amplitude for peak I of n-type samples is larger than that of peak Ⅱ. Oppositely, for p-type samples, the intensity change amplitude of peak I is smaller than that of peak Ⅱ. Note that except the position of peak I of p-type sample in Fig. 5(b), the evolution of the PL fit peak position and intensity of both n- and p-type samples in Figs. 5(b) and 5(c) also show nonlinear behavior, and the turn point always locates at the sample with the medium doping level.

Compared Figs. 4 and 5, it can be found that the FTIR intensity evolution of the Si–O–Si bond in Fig. 4 is coincidence with the PL intensity evolution in Fig. 5, not only the total PL spectra, but also the two fit peaks. This strongly indicates that the Si–O–Si bond structure in nc-Si is a main recombination center to the PL spectra in this study.[2] Another possible recombination center is the carbon related bonds as shown in Fig. 4. Since there are many kinds of carbon related bonds as shown in Fig. 4, and the FWHM of peak Ⅱ is broader than peak I in Fig. 5, we tentatively suggest that peak Ⅱ is mainly contributed by the recombination centers of the carbon related bonds, while peak I is originated from the Si–O–Si bonds. Additionally, if the carbon related recombination centers are mainly contributing to peak Ⅱ, there are two possible ways they are excited: one is by direct excitation, and the other is by energy transfer from the Si–O–Si related recombination centers. It can be compared between Figs. 4 and 5 that for n-type samples the PL intensity evolution of peak Ⅱ in Fig. 5(c) is coincident with the carbon related bond intensity evolution in Fig. 4, while for p-type samples the PL intensity of peak Ⅱ in Fig. 5 changes in an inverse way as compared with the carbon related bond intensity evolution in Fig. 4. This probably indicates that peak Ⅱ comes not only from the direct excitation of the carbon related bonds but also from the energy transfer from Si–O–Si bonds to carbon related bonds. It can be deduced that if the energy transfer from Si–O–Si dominates the process, the PL intensity evolution is probably originated from the Si–O–Si bond intensity as shown in Fig. 4 for p-type samples.

In conclusion, we have presented some of the doping mechanism and PL feature for a series of doped nc-Si prepared from both n- and p-type silicon wafers by mechanochemical synthesis. The detail doping mechanism is complex and depends on the doping types (n- or p-type). The nc-Si samples show different levels of doping effect, oxidation and carbon bond passivation, and the evolution is nonlinear dependent on the original doping levels of the silicon wafers. We suggest that the doping atoms on or close to the surface of nc-Si will hinder or disturb the process of the surface

functionalization. We also suggest that there are dangling bonds originating from the doping impurity diffusion, which provide the possibility to combine with oxygen. All the samples show double-peak ultraviolet PL features, including the intrinsic samples. Oxygen and carbon related bonds have the possibility to contribute to the PL features, while the doping impurities have a slight influence on the PL features.

References

[1] Oliva-Chatelain B L, Ticich T M and Barron A R 2016 *Nanoscale* **8** 1733
[2] Li Y, Qian B, Sui Z and Jiang C 2013 *Appl. Phys. Lett.* **103** 161908
[3] Xie M, Yuan Z, Qian B and Pavesi L 2009 *Chin. Opt. Lett.* **7** 319
[4] Mastronardi M L, Henderson E J, Puzzo D P and Ozin G A 2012 *Adv. Mater.* **24** 5890
[5] Rowe D J, Jeong J S, Mkhoyan K A and Kortshagen U R 2013 *Nano Lett.* **13** 1317
[6] Zhou S, Pi X, Ni Z, Ding Y, Jiang Y, Jin C, Delerue C, Yang D and Nozaki T 2015 *ACS Nano* **9** 378
[7] Lu P, Mu W, Xu J, Zhang X, Zhang W, Li W, Xu L and Chen K 2016 *Sci. Rep.* **6** 22888
[8] Fukata N 2009 *Adv. Mater.* **21** 2829
[9] Heintz A S, Fink M J and Mitchell B S 2007 *Adv. Mater.* **19** 3984
[10] Perego M, Bonafos C and Faniulli M 2010 *Nanotechnology* **21** 025602
[11] Dalpian G M and Chelikowsky J R 2006 *Phys. Rev. Lett.* **96** 226802
[12] Dalpian G M and Chelikowsky J R 2008 *Phys. Rev. Lett.* **100** 179703
[13] Cho E C, Green M A, Conibeer G, Song D, Cho Y H, Sardera G, Huang S, Park S, Hao X J, Huang Y and Dao L V 2007 *Adv. OptoElectron.* **2007** 69578
[14] Xie M, Li D, Chen L, Wang F, Zhu X and Yang D 2013 *Appl. Phys. Lett.* **102** 123108
[15] Hao X J, Cho E C, Flynn C, Shen Y S, Conibeer G and Green M A 2008 *Nanotechnology* **19** 424019
[16] Clark R J, Dang M K M and Veinot J G C 2010 *Langmuir* **26** 15657